Ecological Indicators 94 (2018) 512–519

Contents lists available at ScienceDirect

Ecological Indicators

journal homepage: www.elsevier.com/locate/ecolind

A null model for assessing the cover-independent role of bare soil connectivity as indicator of dryland functioning and dynamics

Francisco Rodríguez[a], Ángeles G. Mayor[b], Max Rietkerk[c], Susana Bautista[d,*]

[a] Department of Applied Mathematics, University of Alicante, Apdo. 99, 03080 Alicante, Spain
[b] Institut des Sciences de l'Evolution de Montpellier (ISEM), Université de Montpellier, CNRS, IRD, EPHE, CC065, 34095 Montpellier cedex 5, France
[c] Department of Innovation, Environmental and Energy Sciences, Copernicus Institute for Sustainable Development and Innovation, Utrecht University, P.O. Box 80155, 3508 TC Utrecht, The Netherlands
[d] Department of Ecology, University of Alicante, Apdo. 99, 03080 Alicante, Spain

ARTICLE INFO

Keywords:
Connectivity
Drylands
Early-warning signals
Flowlength
Functional indicators
Spatial pattern
Vegetation cover

ABSTRACT

Recent research has identified the connectivity of the bare-soil interpatch areas as a key pattern attribute that controls resource conservation and structure-function feedbacks in dryland ecosystems, and several indices have been developed for this attribute. We aimed to characterize the dependence of bare-soil connectivity on vegetation cover and provide a null model that helps differentiate the independent roles of vegetation pattern and cover in hydrological connectivity and dryland functioning. Using a simple hydrological connectivity index, Flowlength, we developed explicit theoretical expressions for its expected value and variance under a null model of random vegetation cover distribution and constant slope. We also obtained the expected value of Flowlength for a model including an aggregation parameter. We found a non-linear inverse relationship between bare-soil connectivity and vegetation cover, which accounts for sharp increases in runoff and sediment yield for low cover values. The expressions for the mean values and standard errors for the random model allow the construction of confidence intervals, and thus testing for deviations from the null random model in experimental data. We found that positive deviations of Flowlength from the expected values, either under random or aggregated-pattern null models, sharply increase before transitions to a degraded state in a spatially-explicit dryland vegetation model, suggesting that an extraordinary increase in bare-soil connectivity may lead to unavoidable degradation. Our results show that increased deviation from the expected cover-dependent bare-soil connectivity may serve as indicator of ecosystem functional status and imminent transitions.

1. Introduction

Dryland vegetation is commonly structured in vegetation patches interspersed within a matrix of bare (or poorly vegetated) soil. The spatial pattern of vegetation patches and bare-soil interpatches is tightly linked to dryland ecosystem functioning (Ludwig and Tongway, 1995; Aguiar and Sala, 1999; Bautista et al., 2007; Moreno-de las Heras et al., 2012; Puttock et al., 2013; Mayor et al., 2016), and may undergo major changes in response to environmental variability (von Hardenberg et al., 2001; Rietkerk et al., 2004; Barbier et al., 2006; Meron, 2016). Accordingly, several spatial-pattern metrics have been proposed as indicators of dryland functioning (e.g., Tongway and Hindley, 2004; Ludwig et al., 2007a; Mayor et al., 2008), and as early warning signals of catastrophic shifts and desertification (e.g., Kéfi et al., 2007a, 2014; Guttal and Jayaprakash, 2009; Dakos et al., 2010; Corrado et al., 2014).

A number of theoretical and empirical works have pointed to the connectivity of the bare-soil interpatch areas as the key pattern attribute that drives the redistribution and conservation of resources in dryland ecosystems and landscapes (Ludwig and Tongway, 1995; Boer and Puigdefábregas, 2005; Ludwig et al., 2007b), influencing dryland vulnerability to environmental pressures (Mayor et al., 2013). Connectivity has been presented as an organizing concept (Okin et al., 2015) that relates to spatial interactions and feedbacks across scales and explains many patterns and processes observed in drylands. In particular, the connectivity and size of the bare-soil areas modulate the reallocation of water and other resources from source areas to vegetation patches (Espigares et al., 2013; Urgeghe and Bautista, 2015), which is considered to control the structure and function of drylands worldwide (Shachak et al., 1998; Ludwig et al., 2005; Yu et al., 2008). Moreover, changes in landscape-scale connectivity that increase ecosystem leakiness beyond critical thresholds are associated with dryland

* Corresponding author.
E-mail address: s.bautista@ua.es (S. Bautista).

http://dx.doi.org/10.1016/j.ecolind.2017.10.023
Received 29 January 2017; Received in revised form 20 September 2017; Accepted 14 October 2017
Available online 26 October 2017
1470-160X/

degradation and desertification (Ludwig et al., 2007b; Turnbull et al., 2008; Moreno-de las Heras et al., 2012), which suggests that changes in the structural connectivity of dryland landscapes could provide a good indicator of state transitions (Okin et al., 2009; Mayor et al., 2013; Zurlini et al., 2014).

Bare-soil connectivity is dependent on vegetation cover, as it is the case for many other pattern properties (Gardner et al., 1987). Vegetation cover is the most simple and widely used indicator of dryland ecosystem functioning (Elwell and Stocking, 1976; Herrick et al., 2005; Maestre and Escudero, 2009; De Keersmaecker et al., 2015), and has proven to be a good indicator of dryland resilience and potential for recovery after disturbances (Bestelmeyer et al., 2013). However, it has been shown that pattern-based metrics capture important additional information relative to vegetation cover measurements that could help to better define the ecosystem functional state and anticipate transitions. For example, for a given vegetation cover value, the larger and fewer the vegetation patches, the larger the interpatch bare-soil connectivity, and the larger the runoff and sediment yield (Bautista et al., 2007). For a large set of drylands sites across the globe, Berdugo et al. (2017) found that abrupt changes in ecosystem multifunctionality were best captured by the patch-size distribution of vegetation patches than by the total vegetation cover. The dependence of vegetation pattern on vegetation cover makes it difficult to disentangle their relative role in dryland functioning. Null models that represent the expected theoretical relationships between bare-soil connectivity and vegetation cover would allow assessing the independent effect of both properties on dryland functioning, providing a deeper understanding of the processes at work. This kind of null models could also be used to develop spatial metrics that provide early warning signals of desertification. Using a simple connectivity metric, here we aim to provide such theoretical relationships, illustrating their potential to assist in the assessment and analysis of dryland functioning and dynamics.

Existing metrics for bare-soil connectivity typically aim to capture the potential hydrological connectivity of bare-soil interpatches (Ludwig et al., 2002, 2007a; Mayor et al., 2008; Puttock et al., 2013). Mayor et al. (2008) developed Flowlength, a simple metric that specifically measures the accumulated length of the potential runoff pathways considering both vegetation pattern and topography. Flowlength is calculated as the average of the pathway lengths from all the pixels in a raster-based vegetation map of the area of interest. For each pixel in the map, the potential pathway for runoff is determined following the steepest descent direction until a runoff sink (i.e., vegetation pixel or topographic depression) or a boundary pixel is reached. Flowlength has been successfully tested against water and soil loss measurements at the slope and catchment scales, showing a positive linear relationship with runoff and sediment yield (Mayor et al., 2008). This metric has received much attention in both hydrological and ecological research (e.g., Cantón et al., 2011; Larsen et al., 2012; Moody et al., 2013; Puttock et al., 2013; Wu et al., 2016), and is being increasingly used to quantifying hydrological connectivity and estimating ecosystem functioning in dryland landscapes (Moreno-de las Heras et al., 2012; Muñoz-Robles et al., 2013; Liu et al., 2013; Mayor et al., 2013).

Here we aim to (1) provide explicit theoretical expressions for the expected value of the Flowlength index under a complete spatial random cover distribution and for a simple aggregated-pattern model, (2) illustrate the use of this kind of null models to disentangling the independent role played by plant cover and pattern in dryland functioning, and (3) assess the potential of using the deviation from the null model as indicator of ecosystem functional status and transitions.

2. Methods

2.1. Models

We develop explicit theoretical expressions for the expected value and variance of the Flowlength index under a null model of constant slope and complete spatial random cover distribution (hereafter random model). To illustrate the effects of non-random patterns on bare-soil connectivity, we also obtain the expected value of the Flowlength index for a simple model including an aggregation parameter, which allows for local correlations that result from processes such as local facilitation of vegetation (Kéfi et al., 2007b). For details on the computation of the Flowlength index see Mayor et al. (2008). We consider a grid of cells or pixels of size ps in a planar slope with angle θ, so that the length of the flowpath (d_s) from a pixel to the neighboring downslope pixel is $d_s = ps/\cos(\theta)$. Since flow can only progress downslope, the analysis can be restricted to a column of 1-pixel width and L-pixels length along the slope. The strategy to derive the analytical expressions is to obtain recurrence relations for the expected values in terms of the length of the slope (L), which are solved and simplified (see Appendix A).

Using the theoretical expressions for the expected values provided in the next section (Eqs. (1)–(4)), estimations of the Flowlength index for real or simulated plots under the null models of random cover or locally aggregated cover are obtained (denoted eFLrdm and eFLagg, respectively). For a particular 2-dimensional plot with constant slope, consisting of M columns of length L, eFLrdm is calculated using Eq. (1), where the parameter p is estimated as the mean value of vegetation cover in the plot. The standard error for the estimation of eFLrdm can be calculated using Eqs. (1) and (2), and considering the plot as a sample of size M. To calculate eFLagg, Eq. (4) is used, where the aggregation parameter α_b (aggregation parameter for bare soil) is estimated from the frequency of pairs of contiguous bare pixels in the plot, computed column-wise, and the plot mean vegetation cover.

2.2. Null models versus observed connectivity and hydrological functioning

To illustrate deviations from the null model in real landscapes, we used images extracted from Google Earth imagery for two areas with contrasting vegetation patterns: banded patterns in Mulga landscapes, Northern Territory, Australia, and spotted patterns in Chihuahuan Desert shrublands and Semidesert grasslands, Southeastern Arizona, USA (Fig. S1, Supplementary material). Both areas have received attention in previous studies on pattern-function relationships and dryland degradation (e.g., Brown et al., 1997; Valone et al., 2002; Witford, 2002; Saco et al., 2007; Moreno-de las Heras et al., 2012). For each site, we extracted six square images (plots) that represented a gradient in vegetation cover. The plots from Arizona were ~150 m × 150 m in size, while the plots from the Mulga landscapes were of larger size (~800 m × 800 m) in order to capture the characteristic larger scale of the banded patterns. All plots had southern orientation, similar slope angles, and quite homogeneous topography. The plots were aligned with the maximum slope; the mean slope angle for each plot was also derived from Google Earth by considering the plot length and the elevation change along the plot. The extracted plot images were transformed into black (vegetation patches) and white (bare soil interpatches) binary maps through thresholding, using the graythresh function from Matlab (copyright *The Mathworks Inc.*), with similar dimensions in pixels (~800 × 800 pixels). From these maps, we estimated total vegetation cover and computed the observed Flowlength values for each plot and landscape type (Mayor et al., 2008), re-scaling them to unit length along the slope. We then assessed the deviations of the observed Flowlength values from the theoretical Flowlength-cover relationship estimated assuming a random distribution of vegetation patches on an idealized square plot of 800 × 800 pixels. We computed the expected value and also upper and lower limits (mean ± 10 times the standard error of the mean), providing a conservative 99% confidence interval under any distribution (Tschebyscheff's inequality, e.g., Rényi, 2007, p. 373).

To illustrate how the theoretical expressions for the expected values of Flowlength allow discriminating between cover and pattern effects on dryland functioning, we analyzed the covariation between available

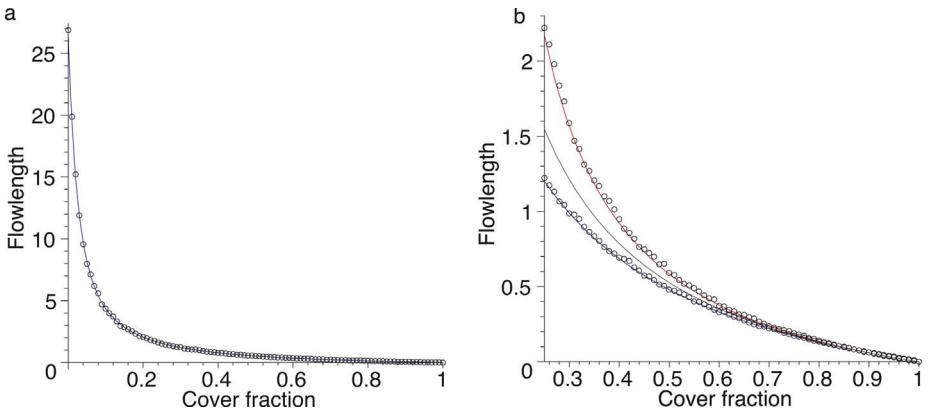

Fig. 1. Expected value of Flowlength as function of vegetation cover, for a constant slope plot ($L = 100$, $ps = 0.5$, $\theta = \pi/9$, $d_s = 0.5321$). Theoretical functions (lines), and simulated results (circles), obtained from a set of 500 simulations for each cover value (for cover fraction varying by 0.01 increments). Left: Random cover distribution. Right: Different values of the aggregation parameter α_b: $\alpha_b = 0.9$ (lower line, blue), $\alpha_b = 1.1$ (upper line, red), and $\alpha_b = 1$ (reference intermediate line, corresponding to the random model). (For interpretation of the references to color in this figure legend, the reader is referred to the web version of this article.)

records of runoff and sediment yield produced on nine experimental plots (16 m^2) over a four-year monitoring period (Bautista et al., 2007) and the expected and observed Flowlength values estimated from available binary (vegetation – bare soil) maps of each plot. For all plots, we used a common baseline DEM with no microtopography, simulating an idealized planar hillslope with a slope angle of 25° (average value for the nine plots). We used Pearson correlation coefficients to analyze the bivariate correlations between total runoff, total sediment yield, observed Flowlength (FL), expected FL for random vegetation distribution (eFLrdm) and expected FL for a locally-aggregated distribution (eFLagg).

2.3. Deviations from null models as early warning signals

To assess the potential of using the deviations from the null models for Flowlength as functional indicators and warning signals of catastrophic shifts, we compared observed FL and estimated eFLrdm and eFLagg values for the outputs of a well-known spatially explicit dryland model (hereafter CA model) that exhibits catastrophic transitions (Kéfi et al., 2007b). The model is a stochastic cellular automaton that represents a dryland ecosystem by a grid of vegetated, empty or degraded cells. Empty cells represent bare soil that is suitable for plant colonization, while degraded cells represent eroded soil that cannot be colonized by vegetation. The model represents local facilitation (i.e., the positive effect of vegetation on its local environment) as an increased regeneration rate of degraded cells, from degraded to empty, when they are contiguous to vegetated cells. The colonization rate of empty cells depends on a parameter (b) that reflects the external pressure on the system. The parameters and parameter values considered in the model simulations are summarized in Table S1 (Supplementary material). We run simulations for combinations of parameter values previously used by Kéfi et al. (2007a) that represented increased external pressure on the dryland system, eventually resulting in catastrophic transitions in the state variable. Each simulation was run until the bare-soil connectivity of the system reached equilibrium (i.e., steady-state conditions for Flowlength). For each steady-state lattice that resulted from the simulations, we estimated the observed FL value and calculated its relative deviation from the expected eFLrdm and eFLagg as (FL-eFLrdm)/eFLrdm and (FL-eFLagg)/eFLagg, respectively. The simulations started with a random distribution of 90% of vegetated cells, 5% of empty cells, and 5% of degraded cells, and were carried out on grids of 100 × 100 cells with a cell-size of 0.5 m. We used an idealized planar topography with an angle of 20° for the calculation of FL.

3. Models and results

3.1. Random model

For our random null model, we consider that each pixel has probability p of being covered by vegetation, and $1 - p$ of being bare, independently of all other pixels.

Let $F(L)$ be the expected value of the flowlength sum for a column of size L when $d = 1$, so that the expected value of Flowlength, denoted $E(Fl)$ or simply Fl, is $Fl = d_s \times F(L)/L$. Then, a recurrence relation in terms of L can be obtained and solved (see Appendix A), and hence it can be shown that, under the random null model, the expected value of the Flowlength index as a function of the vegetation cover p is given by

$$E(\mathrm{Fl}) = \frac{(1-p)(\mathrm{pL} - (1-p)(1-(1-p)^L))d_s}{p^2 L}. \quad (1)$$

Note that, from (1), $\lim_{p\to 0}(\mathrm{Fl}) = d_s(L+1)/2$, which is the maximum value of Flowlength, corresponding to $p = 0$.

Following a similar approach, an explicit expression for the expected value of the square of Flowlength can also be derived (see Appendix A),

$$E(\mathrm{Fl}^2) = \frac{(1-p)(p^2(1-p)(L+1)^2 + p^2 L - 6(1-p) + (1-p)^{L+1}(p^2(2L^2-1) + 6\mathrm{pL} + 6))d_s^2}{p^4 L^2}. \quad (2)$$

Thus, from (2) and (1), the variance of the Flowlength index can be computed as $V(Fl) = E(Fl^2) - E(Fl)^2$, and, consequently, also its standard deviation, $sd(Fl)$, and the standard error of the mean can be obtained. Plots of $E(Fl)$ and $sd(Fl)$ versus p, for particular values of L and d_s, are shown in Fig. 1 (left) and Fig. S2 (Supplementary material).

3.1.1. Model with aggregation parameter

We consider now a simple model allowing for non-independence between contiguous cells. In this model, the probability of a pair of contiguous pixels being both vegetated will be $p_{++} = \alpha_v p^2$, and of both being bare will be $p_{--} = \alpha_b(1-p)^2$. Note that there is only one independent parameter in the model, since the fact that p is the probability of a cell being covered implies that α_v and α_b satisfy the relation

$$p(1 - \alpha_v p) = (1-p)(1 - \alpha_b(1-p)), \quad (3)$$

which also follows immediately from the fact that the probability of two contiguous pixels being in different states, p_{+-}, must be the same irrespectively on how it is computed.

When $\alpha_v > 1$ there is aggregation of the vegetated cells, in which case, from (3), it also holds that $\alpha_b > 1$, representing aggregation of the bare pixels. When $\alpha_v < 1$, so that also $\alpha_b < 1$, the patterns of covered and bare cells show a certain degree of regularity, while when $\alpha_v = \alpha_b = 1$ the random model is recovered.

Writing $q = \alpha_b(1-p)$, it can be shown (see Appendix A) that the expected value of the Flowlength, expressed in terms of α_b, is given by

$$E(\mathrm{Fl}) = \frac{(1-p)((1-q)L - q(1-q^L))d_s}{(1-q)^2 L}. \quad (4)$$

Using the relation (3), an equivalent expression in terms of α_v can be written.

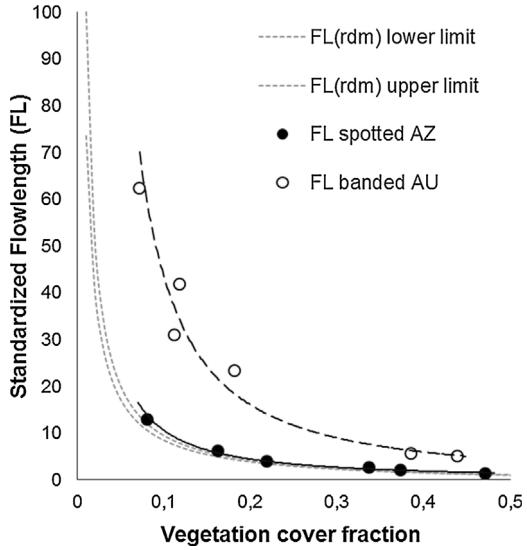

Fig. 2. Variation in observed Flowlength (FL) versus vegetation cover fraction, and fitted non-linear trends, for two dryland landscapes with contrasting vegetation pattern: banded patterns in Mulga landscapes, Northern Territory, Australia (open circles, long-dashed line) and spotted patterns in Chihuahuan Desert shrublands, Arizona, USA (filled circles, solid line). The upper and lower limits of the confidence interval for the expected FL-cover relationship under a null model of random distribution of vegetation cover are shown. Standardized FL values are re-scaled values to unit length along the slope.

The effect of non-random patterns on the Flowlength index, for this simple model, is illustrated in Fig. 1 (right) and Fig. S3 (Supplementary material). We note that the values of the aggregation parameters are constrained depending on the vegetation cover p. Intuitively, when cover is very low, α_b is necessarily close to 1, as most contiguous pixels are both bare, and similarly for α_v when p is close to 1. More precisely, since it holds that $1 - 2p < p_{--} \leq 1 - p$, it follows that

$$\frac{1-2p}{(1-p)^2} < \alpha_b \leq \frac{1}{1-p}, \tag{5}$$

and corresponding bounds hold for α_v.

3.2. Using the null models to develop indicators of dryland functioning and dynamics

Fig. 2 illustrates the use of the theoretical relationship between FL and vegetation cover for the assessment of connectivity patterns as compared with the null model of random cover distribution. For two contrasting dryland landscapes, comparisons between observed FL values and the expected FLrdm-cover relationship showed a higher aggregation of the bare-soil pattern than the expected pattern from a random distribution of vegetation, yet both landscapes exhibited the same kind of non-linear inverse relationship between vegetation cover and FL (Fig. 2). Deviations from a random pattern were much larger for the banded pattern of Mulga landscapes than for the spotted patterns of the Chihuahuan shrublands, the latter including plots with vegetation patterns than cannot be distinguished from random distributions.

Bivariate relationships between vegetation cover, observed FL, expected FL under null models for random and aggregated cover distributions, and measured runoff and sediment yields (Fig. 3) illustrate the independent role of vegetation cover and pattern as control factors of dryland hydrological functioning. Both total runoff and sediment yield produced on nine experimental plots over a 4-year period were positively correlated with FL and eFLagg. Vegetation cover, which slightly varied between plots and was highly correlated with eFLrdm, showed no significant correlation with runoff or sediment yield.

Fig. 4 shows the variation of the state variable (vegetation cover) at equilibrium predicted by the CA model for a gradient of initial environmental conditions (b) and a moderate disturbance value ($m = 0.2$) together with the deviations of the bare-soil connectivity for each equilibrium state relative to the null models for random and aggregated cover distributions. For the conditions simulated, decreasing values of b resulted in gradually decreasing vegetation cover at equilibrium, with an abrupt transition between a vegetated state, with cover values around 20%, and a degraded state (with no vegetation cover) occurring for $b = 0.55$. The relative deviations of FL from both the random and aggregated null models slightly varied for a wide range of decreasing b values, but they sharply increased in the proximity of the shift between the vegetated and the degraded states, which indicates an increased aggregation of the bare-soil gaps (Fig. 4, top panel) beyond the values expected for either random cover distributions or aggregated patterns based on local facilitation. This results were consistent for a variety of disturbance (m) values (Fig. S4; Supplementary material).

4. Discussion

Dryland vegetation can respond to external stress by reorganizing its spatial structure (von Hardenberg et al., 2001; Rietkerk et al., 2004), which in turn influences ecosystem functions (Bautista et al., 2007; Moreno-de las Heras et al., 2012). Both vegetation cover and spatial pattern reflect changes in dryland functioning and ecosystem state, yet they may capture different processes and respond differently to control factors, and therefore exhibit different potential as indicators and early warning signals (Berdugo et al., 2017). The theoretical expressions presented here provide null models that allow disentangling the effects of vegetation cover and vegetation spatial pattern. Furthermore, using model simulations of a spatially-explicit dryland ecosystem model that exhibits alternative stable states, we found sharply increasing positive deviations from the expected null-model values in the proximity of a bifurcation, which points to the potential of these deviations as early warning signals of state transitions in drylands.

Bare-soil connectivity depends on both vegetation cover and pattern. Non-linear dependence on cover of Flowlength and other bare-soil connectivity metrics is supported by empirical field data and model outputs for a range of vegetation patterns, from spotted to banded (e.g., Ludwig et al., 2007b; Moreno-de las Heras et al., 2012; Mayor et al., 2013). Our results illustrate how the expected values and confidence intervals for Flowlength under a null model of random cover distribution can be used to assess and compare the contribution of vegetation pattern to bare-soil connectivity for a variety of landscapes and/or a variety of conditions within a landscape type. For example, the characteristic large connectivity of bare-soil gaps in Mulga landscapes is reflected by large deviations from the null model, particularly for vegetation cover values between 10% and 20%. Conversely, for a wide vegetation cover range in Chihuahuan Desert shrublands, bare-soil connectivity did not show major deviations from the null model, indicating that the spatial pattern of vegetation, and therefore the processes underlying pattern formation, did not contribute to shape bare-soil connectivity beyond the role played by vegetation cover alone. Along these lines, the expressions obtained in this work also allow analyzing the independent role of vegetation cover and pattern as control factors of dryland functioning. We illustrated this potential using data from experimental runoff plots that showed contrasting vegetation spatial pattern and low variation in vegetation cover. Accordingly, the comparative analysis of the explanatory value of the expected and measured Flowlength, and vegetation cover values revealed that total runoff and sediment yield produced on these plots mostly depended on the spatial pattern of vegetation, which in turn mostly reflected a local aggregation pattern.

Some properties of connectivity indices, evidenced by the expressions provided in this paper for the Flowlength index, may help clarify the relations between hydrological behavior, vegetation cover, and vegetation pattern. Assuming that connectivity indices as Flowlength are good indicators of hydrological functions, the non-linear

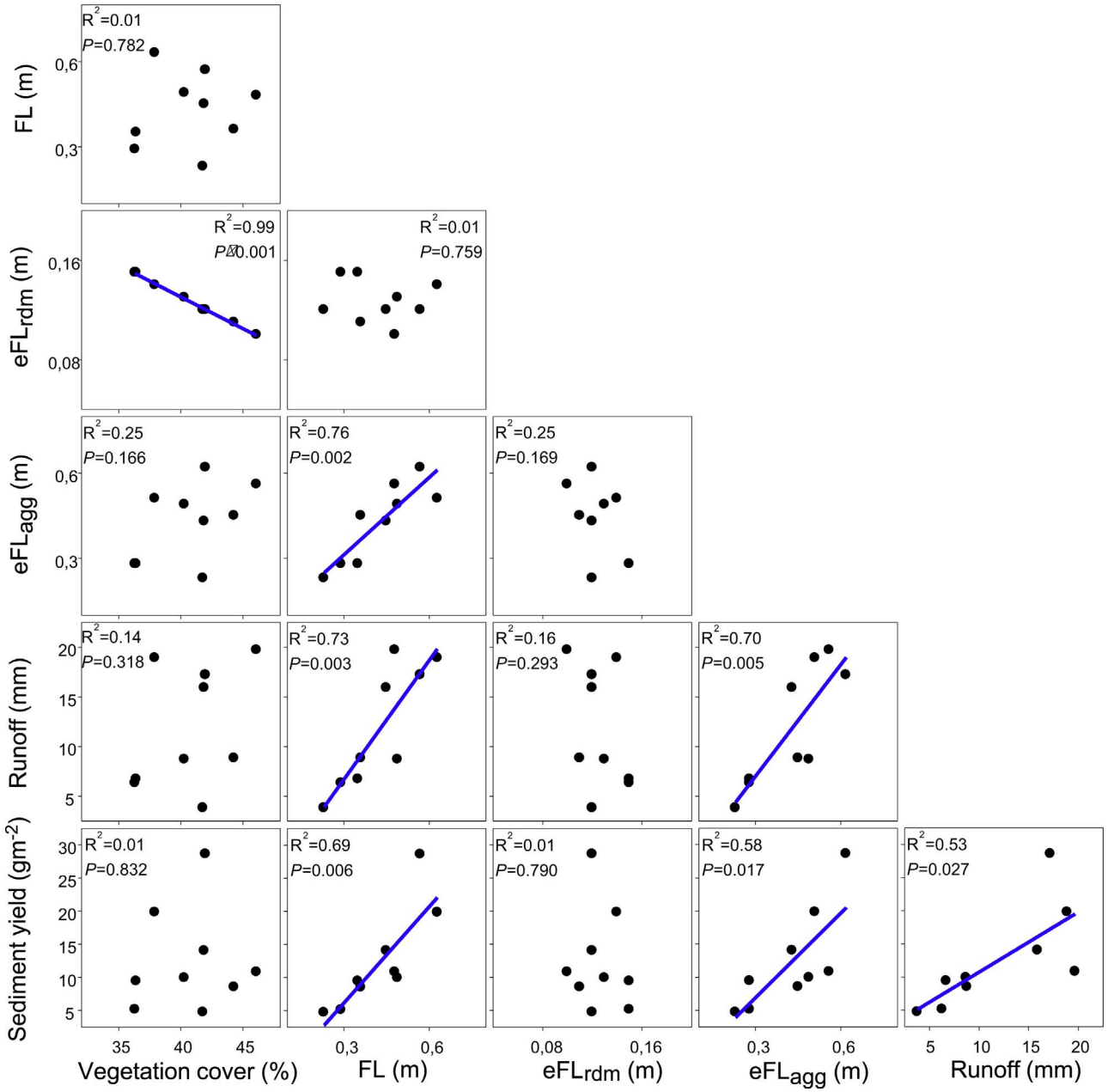

Fig. 3. Bivariate relationships between vegetation cover, observed Flowlength (FL), expected FL under null models for random (eFLrdm) and aggregated (eFLagg) cover distributions, and measured runoff and sediment yields on nine experimental plots over a four-year monitoring period; original data from Bautista et al., 2007. Results (R^2 and *p*-values) from regression analysis are shown; regression lines are plotted for significant regressions.

dependence of connectivity on vegetation cover, reflected on Eqs. (1) and (4), and illustrated in Fig. 1, accounts for sharp changes in runoff or sediment yields for low cover values, without having to invoke threshold phenomena as control processes. Non-linear relationships between soil erosion and plant cover are commonly reported from empirical assessment (Elwell and Stocking, 1976; Francis and Thornes, 1990; Abrahams et al., 1995; Zuazo and Rodriguez, 2008), which may basically reflect the expected non-linear dependence on plant cover of bare-soil connectivity. It nevertheless remains that this type of non-linear behavior for resource loss may potentially induce critical transitions between ecosystem states (Rietkert et al., 1997; Mayor et al., 2013).

Our results suggest that the degree to which the observed Flowlength values deviate from the expected values for a random vegetation cover distribution might be used as warning signals of the proximity to transitions towards degraded states in drylands. A decrease in vegetation cover entails a non-linear increase in bare-soil connectivity, as defined by the theoretical expressions provided for Flowlength. Positive deviations of Flowlength from the values expected for a random cover distribution reflect an aggregated vegetation pattern; positive deviations from the values expected for a simple aggregate-pattern model indicate more complex aggregate patterns than simple local correlations. Sharp increases in both these deviations suggest additional, heightened aggregation connectivity of bare-soil areas. The resulting increased spatial coherence between bare-soil neighboring units is consistent with an increased recovery time from local perturbations (e.g., death or removal of vegetation units) as the system approaches a state transition (Dakos et al., 2010), a phenomenon that underlies a number of early warning signals proposed in the literature (Scheffer et al., 2009; Kéfi et al., 2014). The escalated bare-soil connectivity can be explained by positive feedbacks between soil degradation, resource loss and reduced plant establishment in bare-soil

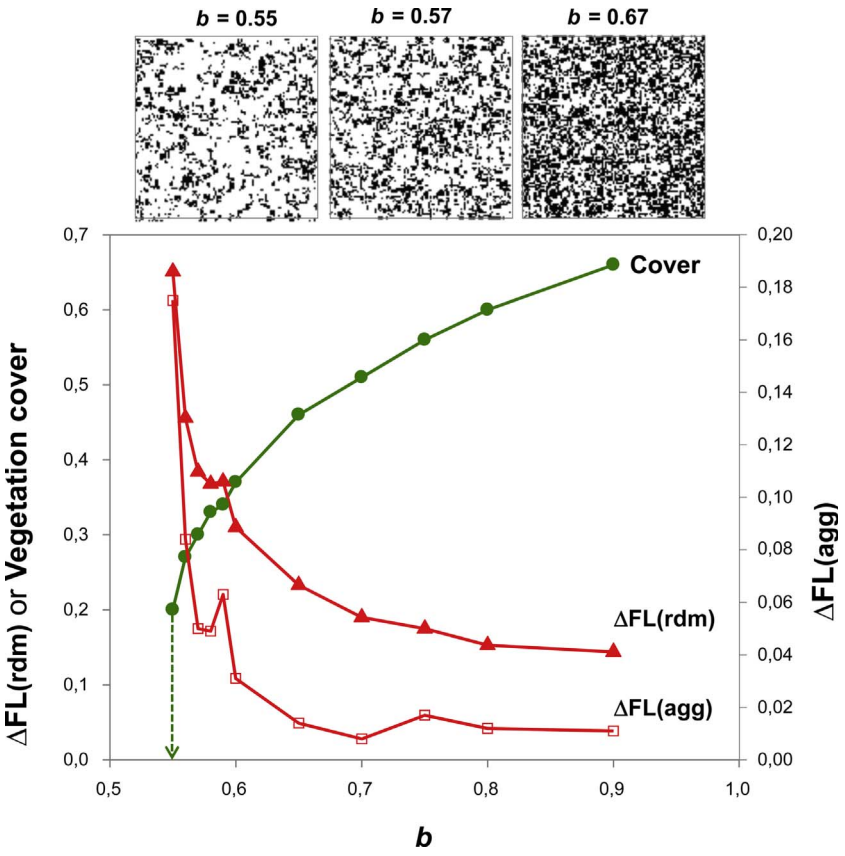

Fig. 4. Values at equilibrium in simulations for vegetation cover (circles, green line) and for the relative differences between Flowlength and the expected values for random (ΔFL(rdm), triangles, upper red line) or aggregated cover (ΔFL(agg), squares, lower red line), for $m = 0.20$ in response to changing environmental conditions (b). Top: Snapshots of the system at the end of the simulation (black: vegetated cells; white: bare cells). (For interpretation of the references to color in this figure legend, the reader is referred to the web version of this article.)

interpatches (Mayor et al., 2013). It could result from the fragmentation of big vegetation patches once local facilitation cannot counterbalance the effects of increasing environmental stress and disturbance-driven mortality (Kéfi et al., 2007b). Although we show here that deviations from the expected cover-dependent bare-soil connectivity are promising indicators, testing their potential as early warning of state transitions requires further research, including the analysis of these deviations across environmental stress gradients in real landscapes.

5. Conclusions

In a dryland context, with characteristic patchy vegetation and landscape heterogeneity, connectivity stands out as an emerging property that links ecosystem structure and functions across scales, and contributes to feedbacks that can explain transitions to degraded states (Mayor et al., 2013; Okin et al., 2015; Zurlini et al., 2014). We developed null models for estimating the expected value of a well-known connectivity index, the Flowlength index, under both random and locally-aggregated vegetation cover distributions, providing a tool for disentangling the role of vegetation cover and pattern in dryland functioning, and crystalizing the value of bare-soil connectivity as functional indicator into a potential early warning signal of imminent degradation. The null models developed here are specific for Flowlength, yet similar models could be developed for a variety of connectivity metrics. Flowlength exhibits a non-linear inverse dependence on vegetation cover. The expressions for the mean values and standard errors for the random model allow the construction of asymptotic confidence intervals, as well as testing for deviations from the null model in experimental data, and thus may help discriminate between cover and pattern effects. The dependence of Flowlength on pattern as captured in a simple aggregated-pattern null model may also provide a reference to separate expected effects of local correlations from more complex aggregate patterns. The expressions obtained in this work may be of use in ecohydrological models that consider the impact of resource redistribution and loss in ecosystem functions and dynamics. These expressions can be directly incorporated into deterministic models, and they can also help understand spatially-explicit models, as the one considered in Mayor et al. (2013), by allowing analysis of mean-field or pair approximations (Kéfi et al., 2007a). Lastly, sharp positive deviations of Flowlength from the expected values for either random or aggregated cover occur before bifurcations in a spatially-explicit dryland ecosystem model. Such behavior suggests that a sort of enhanced bare-soil coalescence process precedes transitions, and points to the potential of these deviations as early warning signal of an impending transition towards a degraded state.

Acknowledgements

This work was supported by the research projects FEEDBACK (CGL2011-30515-C02-01) and DRYEX (CGL2014-59074-R), funded by the Spanish Ministry of Economy and Competitiveness, and the EC-funded project CASCADE (GA283068). FR and SB acknowledge financial support from the “Programa Estatal de Promoción del Talento y su Empleabilidad en I+D+i, Subprograma Estatal de Movilidad, del Plan Estatal de Investigación Científica y Técnica y de Innovación 2013-2016”, (PRX14/00691 and PRX16/00583), funded by the Spanish Ministry of Education, Culture and Sports (MECD). FR also acknowledges financial support from the Valencia Regional Government, Generalitat Valenciana (BEST/2014/285). AGM was supported by the EC-funded Marie Skłodowska-Curie Action ECOHYDRY (GA660859).

Appendix A. Theoretical expressions for the Flowlength index

A.1 Random model

Assume that $F(l)$, the expected values of the flowlength sums for columns of size l when $d_s = 1$, are known for $l = 1, \ldots, L-1$, where $F(1) = 1 - p$. Taking into account that the contribution to the flowlength sum is zero for a vegetated pixel, and that it is $k(k+1)/2$ for a stretch of k bare pixels delimited by vegetated ones, the following recurrence relation for $F(L)$ can be deduced,

$$F(L) = \mathrm{p}\,\mathrm{F}(L-1) + \sum_{k=1}^{L-2} p(1-p)^k \left(\frac{k(k+1)}{2} + F(L-1-k) \right) + p(1-p)^{L-1}\frac{(L-1)L}{2} + (1-p)^L \frac{L(L+1)}{2}. \tag{A.1}$$

This difference equation can be solved, for instance, by transformation into a matrix equation. To this end, set $F(0) = 1$ and consider the vectors $\mathrm{F} = [F(L), F(L-1), \ldots, F(0)]^T$ and $\mathrm{V} = [0{\cdot}1/2,\ 1{\cdot}2/2, \ldots, L(L+1)/2]^T$, where the superindex T denotes the transpose, and the $(L+1) \times (L+1)$ matrices $\mathrm{A} = [A_{ij}]$ and $\mathrm{B} = [B_{ij}]$, where $A_{ij} = p(1-p)^{j-i-1}$ for $i < j$ and $A_{ij} = 0$ otherwise, and $B_{ij} = p(1-p)^{j-1}$ for $j = 1$ and $j < L - i$, $B_{ij} = (1-p)^{j-1}$, for $j = i > 1$, and $B_{ij} = 0$ otherwise. Thus, from (A.1) we are led to the matrix equation $\mathrm{F} = \mathrm{AF} + \mathrm{BV}$, so that, writing I for the identity matrix, one gets $\mathrm{F} = (\mathrm{I} - \mathrm{A})^{-1}\mathrm{BV}$, where the elements of the matrix $\mathrm{C} = (\mathrm{I} - \mathrm{A})^{-1}$ are $C_{ij} = p$ for $i < j$, $C_{ij} = 1$ for $i = j$, and zero otherwise. Hence, an explicit expression for $F(L)$ is obtained,

$$F(L) = \sum_{k=1}^{L-1} \frac{k(k+1)}{2}(2 + (L-k-1)p)p(1-p)^k + \frac{L(L+1)}{2}(1-p)^L, \tag{A.2}$$

which, after computing a closed form of the sum and some simplifications, lead to the compact form for $E(Fl)$ given in (1).

We note that expression (A.2) has a simple interpretation, as it is the sum of Flowlength contributions from all possible stretches of bare cells of size k, either ending in one of the borders or delimited by vegetated cells, weighted by their respective probabilities.

With a similar approach, the following expression can be obtained for the expected value of the square of Flowlength,

$$E(\mathrm{Fl}^2) = \frac{(1-p)^L d^2 (L+1)^2}{4} + \frac{d^2}{L^2}\sum_{k=1}^{L-1}(2 + (L-k-1)p)p(1-p)^k \frac{k^2(k+1)^2}{4} + \frac{d^2}{L^2}\sum_{k=1}^{L-1}(2 + (L-k-1)p)(1-p)^{k+1}\frac{k(k+1)}{2}(L-k-2+(1-p)^{L-k-1}). \tag{A.3}$$

Computing closed forms of the sums in (A.3) and simplifying the results, the expression for $E(Fl^2)$ given in (2) is obtained.

A.2 Model with aggregation parameter

For the model with local dependencies considered in this work, the approach of establishing recurrence relations in terms of L can also be applied, but now it is necessary to work with two different Flowlength sums, depending on the first pixel being bare or vegetated. However, the final resulting expression can be much more easily deduced by making adequate minimal changes in expression (A.2).

The probability for each Flowlength contribution from a stretch of k bare cells is obtained by multiplying the probability of one pixel being bare, $(1-p)$, by the probability of the $(k-1)$ contiguous pixels being also bare, which is now q^{k-1}, where $q = \alpha_b(1-p)$, and either the probability of having two delimitating vegetated pixels, which is $(1-q)^2$, or, for stretches ending in one of the borders and with a vegetated cell in the other end, the probability of finding one vegetated pixel contiguous to a bare one, which is $(1-q)$. Thus, the only changes needed in (A.2) consist in substituting, in each term, all but one of the factors $(1-p)$ by q, and replacing the factors p by $(1-q)$. The resulting expression reads

$$F(L) = (1-p)\left(\sum_{k=1}^{L-1} \frac{k(k+1)}{2}(2 + (L-k-1)(1-q))(1-q)q^{k-1} + \frac{L(L+1)}{2}q^{L-1} \right), \tag{A.4}$$

from which the compact form for $E(Fl)$ given in (4) is obtained.

Appendix B. Supplementary data

Supplementary data associated with this article can be found, in the online version, at http://dx.doi.org/10.1016/j.ecolind.2017.10.023.

References

Abrahams, A.D., Parsons, A.J., Wainwright, J., 1995. Effects of vegetation change on interrill runoff and erosion, Walnut-Gulch, southern Arizona. Geomorphology 13, 37–48.

Aguiar, M.R., Sala, O.E., 1999. Patch structure, dynamics and implications for the functioning of arid ecosystems. Trends Ecol. Evol. 14, 273–277.

Barbier, N., Couteron, P., Lejoly, J., Deblauwe, V., Lejeune, O., 2006. Self organized vegetation patterning as a fingerpint of climate and human impact on semi-arid ecosystems. J. Ecol. 94, 537–547.

Bautista, S., Mayor, A.G., Bourakhouadar, Bellot, J., 2007. Plant spatial pattern predicts hillslope runoff and erosion in a semiarid Mediterranean landscape. Ecosystems 10, 987–998.

Berdugo, M., Kéfi, S., Soliveres, S., Maestre, F.T., 2017. Plant spatial patterns identify alternative ecosystem multifunctionality states in global drylands. Nat. Ecol. Evol. 1, 0003.

Bestelmeyer, B.T., Duniway, M.C., James, D.K., Burkett, L.M., Havstad, K.M., 2013. A test of critical thresholds and their indicators in a desertification-prone ecosystem: more resilience than we thought. Ecol. Lett. 16, 339–345.

Boer, M., Puigdefábregas, J., 2005. Effects of spatially structured vegetation patterns on hillslope erosion in a semiarid Mediterranean environment: a simulation study. Earth Surf. Proc. Landf. 30, 149–167.

Brown, J.H., Valone, T.J., Curtin, C.G., 1997. Reorganization of an arid ecosystem in response to recent climate change. Proc. Natl. Acad. Sci. U.S.A. 94, 9729–9733.

Cantón, Y., Solé-Benet, A., de Vente, J., Boix-Fayos, C., Calvo-Cases, A., Asensio, C., Puigdefábregas, J., 2011. A review of runoff generation and soil erosion across scales in semiarid south-eastern Spain. J. Arid Environ. 75, 1254–1261.

Corrado, R., Cherubini, A.M., Pennetta, C., 2014. Early warning signals of desertification transitions in semiarid ecosystems. Phys. Rev. E 90, 062705.

Dakos, V., van Nes, E.H., Donangelo, R., Fort, H., Scheffer, M., 2010. Spatial correlation as leading indicator of catastrophic shifts. Theoret. Ecol. 3, 163–174.

De Keersmaecker, W., Lhermitte, S., Tits, L., Honnay, O., Somers, B., Coppin, P., 2015. A model quantifying global vegetation resistance and resilience to short-term climate anomalies and their relationship with vegetation cover. Glob. Ecol. Biogeogr. 24 (5), 539–548.

Elwell, H.A., Stocking, M.A., 1976. Vegetal cover to estimate soil erosion hazard in Rhodesia. Geoderma 15, 61–70.

Espigares, T., Merino-Martín, L., Moreno-de las Heras, M., Nicolau, J.M., 2013. Intensity of ecohydrological interactions in reclaimed Mediterranean slopes: effects of run-off redistribution on plant performance. Ecohydrology 6, 836–844.

Francis, C.F., Thornes, J.B., 1990. Runoff hydrographs from three Mediterranean

vegetations cover types. In: Thornes, J.B. (Ed.), Vegetation and Erosion, Processes and Environments. Wiley, Chichester, pp. 363–384.
Gardner, R.H., Milne, B.T., Turner, M.G., O'Neill, R.V., 1987. Neutral models for the analysis of broad-scale landscape pattern. Landsc. Ecol. 1, 19–28.
Guttal, V., Jayaprakash, C., 2009. Spatial variance and spatial skewness: leading indicators of regime shifts in spatial ecological systems. Theoret. Ecol. 2, 3–12.
Herrick, J.E., Van Zee, J.W., Havstad, K.M., Whitford, W.G., 2005. Monitoring Manual for Grassland, Shrubland, and Savanna Ecosystems. Volume II. Design, Supplementary Methods and Interpretation. U.S. Department of Agriculture, Agricultural Research Station, Las Cruces, New Mexico, USA.
Kéfi, S., Rietkerk, M., Alados, C.L., Pueyo, Y., Papanastasis, V.P., ElAich, A., de Ruiter, P.C., 2007a. Spatial vegetation patterns and imminent desertification in Mediterranean arid ecosystems. Nature 449, 213–217.
Kéfi, S., Rietkerk, M., van Baalen, M., Loreau, M., 2007b. Local facilitation, bistability and transitions in arid ecosystems. Theoret. Popul. Biol. 71, 367–379.
Kéfi, S., Guttal, V., Brock, W.A., Carpenter, S.R., Ellison, A.M., Livina, V.N., Seekell, D.A., Scheffer, M., van Nes, E.H., Dakos, V., 2014. Early warning signals of ecological transitions: methods for spatial patterns. PLOS ONE 9 (3), e92097.
Larsen, L.G., Choi, J., Nungesser, M.K., Harvey, J., 2012. Directional connectivity in hydrology and ecology. Ecol. Appl. 22, 2204–2220.
Liu, Y., Fu, B., Lu, Y., Gao, G., Wang, S., Zhou, J., 2013. Linking vegetation cover patterns to hydrological responses using two process-based pattern indices at the plot scale. Sci. China Ser. D 56, 1888–1898.
Ludwig, J.A., Tongway, D.J., 1995. Spatial organisation of landscapes and its function in semi-arid woodlands, Australia. Landsc. Ecol. 10, 51–63.
Ludwig, J.A., Eager, R.W., Bastin, G.N., Chewings, V.H., Liedloff, A., 2002. A leakiness index for assessing landscape function using remote sensing. Landsc. Ecol. 17, 157–171.
Ludwig, J.A., Wilcox, B.P., Breshears, D.D., Tongway, D.J., Imeson, A.C., 2005. Vegetation patches and runoff-erosion as interacting ecohydrological processes in semiarid landscapes. Ecology 86 (2), 288–297.
Ludwig, J.A., Bastin, G.N., Chewings, V.H., Eager, R.W., Liedloff, A.C., 2007a. Leakiness: a new index for monitoring the health of arid and semiarid landscapes using remotely sensed vegetation cover and elevation data. Ecol. Indic. 7, 442–454.
Ludwig, J.A., Bartley, R., Hawdon, A.A., Abbott, B.N., Mc Jannet, D., 2007b. Patch configuration non-linearly affects sediment loss across scales in a grazed catchment in north-east Australia. Ecosystems 10, 839–845.
Maestre, F.T., Escudero, A., 2009. Is the patch-size distribution of vegetation a suitable indicator of desertification processes? Ecology 90, 1729–1735.
Mayor, A.G., Bautista, S., Small, E.E., Dixon, M., Bellot, J., 2008. Measurement of the connectivity of runoff source areas as determined by vegetation pattern and topography: a tool for assessing potential water and soil losses in drylands. Water Resour. Res. 44, W10423.
Mayor, A.G., Kéfi, S., Bautista, S., Rodríguez, F., Cartení, F., Rietkerk, M., 2013. Feedbacks between vegetation pattern and resource loss dramatically decrease ecosystem resilience and restoration potential in a simple dryland model. Landsc. Ecol. 28, 931–942.
Mayor, A.G., Valdecantos, A., Vallejo, V.R., Keizer, J.J., Bloema, J., Baeza, J., González-Pelayo, O., Machado, A.I., de Ruiter, P.C., 2016. Fire-induced pine woodland to shrubland transitions in Southern Europe may promote shifts in soil fertility. Sci. Total Environ. 573, 1232–1241.
Meron, E., 2016. Pattern formation – a missing link in the study of ecosystem response to environmental changes. Math. Biosci. 271, 1–18.
Moody, J.A., Shakesby, R.A., Robichaud, P.R., Cannon, S.H., Martin, D.A., 2013. Current research issues related to post-wildfire runoff and erosion processes. Earth Sci. Rev. 122, 10–37.
Moreno-de las Heras, M., Saco, P.M., Willgoose, G.R., Tongway, D.J., 2012. Variations in hydrological connectivity of Australian semiarid landscapes indicate abrupt changes in rainfall-use efficiency of vegetation. J. Geophys. Res. 117, G03009.
Muñoz-Robles, C., Tighe, M., Reid, N., Frazier, P., Briggs, S.V., Wilson, B., 2013. A two-step up-scaling method for mapping runoff and sediment production from pasture and woody encroachment on semi-arid hillslopes. Ecohydrology 6, 83–93.
Okin, G.S., Parsons, A.J., Wainwright, J., Herrick, J.E., Bestelmeyer, B.T., Peters, D.C., Fredrickson, E.L., 2009. Do changes in connectivity explain desertification? Bioscience 59, 237–244.
Okin, G.S., Moreno-de las Heras, M., Saco, P.M., Throop, H.L., Vivoni, E.R., Parsons, A.J., Wainwright, J., Peters, D.P.C., 2015. Connectivity in dryland landscapes: shifting concepts of spatial interactions. Front. Ecol. Environ. 13 (1), 20–27.
Puttock, A., Macleod, C.J.A., Bol, R., Sessford, P., Dungait, J., Brazier, E., 2013. Changes in ecosystem structure, function and hydrological connectivity control water, soil and carbon losses in semi-arid grass to woody vegetation transitions. Earth Surf. Proc. Landf. 38, 1602–1611.
Rényi, A., 2007. Probability Theory. Dover Edition (Republication of the Original 1970 Work). Dover Publications, Mineola, NY, USA.
Rietkert, M., van den Bosch, F., van de Koppel, J., 1997. Site-specific properties and irreversible vegetation changes in semi-arid grazing systems. Oikos 80, 241–252.
Rietkerk, M., Dekker, S.C., de Ruiter, P.C., van de Koppel, J., 2004. Self-organized patchiness and catastrophic shifts in ecosystems. Science 305, 1926–1929.
Saco, P.M., Willgoose, G.R., Hancock, G.R., 2007. Eco-geomorphology of banded vegetation patterns in arid and semi-arid regions. Hydrol. Earth Syst. Sci. 11, 1717–1730.
Shachak, M., Sachs, M., Moshe, I., 1998. Ecosystem management of desertified shrublands in Israel. Ecosystems 1, 475–483.
Scheffer, M., Bascompte, J., Brock, W.A., Brovkin, V., Carpenter, S.R., Dakos, V., Held, H., van Nes, E.H., Rietkerk, M., Sugihara, G., 2009. Early-warning signals for critical transitions. Nature 461, 53–59.
Tongway, D.J., Hindley, N., 2004. Landscape Function Analysis: Procedures for Monitoring and Assessing Landscapes. CSIRO Publishing, Brisbane, Australia.
Turnbull, L., Wainwright, J., Brazier, R.E., 2008. A conceptual framework for understanding semi-arid land degradation: ecohydrological interactions across multiple space and time scales. Ecohydrology 1, 23–34.
Urgeghe, A.M., Bautista, S., 2015. Size and connectivity of upslope runoff-source areas modulate the performance of woody plants in Mediterranean drylands. Ecohydrology 8, 1292–1303.
Valone, T.J., Meyer, M., Brown, J.H., Chew, R.M., 2002. Timescale of perennial grass recovery in desertified arid grasslands following livestock removal. Conserv. Biol. 16, 995–1002.
von Hardenberg, J., Meron, E., Shachak, S., Zarmi, Y., 2001. Diversity of vegetation patterns and desertification. Phys. Rev. Lett. 87, 198101.
Witford, W.G., 2002. Ecology of Desert Systems. Academic Press, San Diego, CA, USA.
Wu, Z., Lin, C., Su, Z., Zhou, S., Zhou, H., 2016. Multiple landscape "source-sink" structures for the monitoring and management of non-point source organic carbon loss in a peri-urban watershed. Catena 145, 15–29.
Yu, M., Gao, Q., Epstein, H.E., Zhang, X., 2008. An ecohydrological analysis for optimal use of redistributed water among vegetation patches. Ecol. Appl. 18, 1679–1688.
Zuazo, Z.V.H., Rodriguez, P.C.R., 2008. Soil-erosion and runoff prevention by plant covers. A review. Agron. Sustain. Dev. 28, 65–86.
Zurlini, G., Jones, K.B., Riitters, K.H., Lid, B.-L., Petrosillo, I., 2014. Early warning signals of regime shifts from cross-scale connectivity of land-cover patterns. Ecol. Indic. 45, 549–560.